NANO LETTERS

pubs.acs.org/NanoLett Letter

Nonvolatile Multistate Manipulation of Topological Magnetism in Monolayer CrI_3 through Quadruple-Well Ferroelectric Materials

Peixuan Li, Lei Tao, Xin Jin, Guolin Wan, Jie Zhang, Yan-Fang Zhang, Jia-Tao Sun, Jinbo Pan,* and Shixuan Du*

Cite This: *Nano Lett.* 2024, 24, 2345−2351 Read Online

ACCESS | Metrics & More | Article Recommendations | Supporting Information

ABSTRACT: Nonvolatile multistate manipulation of two-dimensional (2D) magnetic materials holds promise for low dissipation, highly integrated, and versatile spintronic devices. Here, utilizing density functional theory calculations and Monte Carlo simulations, we report the realization of nonvolatile and multistate control of topological magnetism in monolayer CrI_3 by constructing multiferroic heterojunctions with quadruple-well ferroelectric (FE) materials. The $Pt_2Sn_2Te_6/CrI_3$ heterojunction exhibits multiple magnetic phases upon modulating FE polarization states of FE layers and interlayer sliding. These magnetic phases include Bloch-type skyrmions and ferromagnetism, as well as a newly discovered topological magnetic structure. We reveal that the Dzyaloshinskii−Moriya interaction (DMI) induced by interfacial coupling plays a crucial role in magnetic skyrmion manipulation, which aligns with the Fert−Levy mechanism. Moreover, a regular magnetic skyrmion lattice survives when removing a magnetic field, demonstrating its robustness. The work sheds light on an effective approach to nonvolatile and multistate control of 2D magnetic materials.

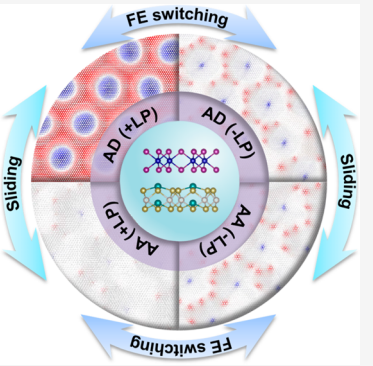

KEYWORDS: *Two-dimensional materials, quadruple-well ferroelectricity, nonvolatile manipulation, magnetic skyrmions, multistate control*

In recent years, two-dimensional (2D) magnetic materials have attracted significant attention owing to their intriguing physical properties, including room-temperature ferromagnetism,[1−4] magnetoelectric coupling,[5−7] spin glass behavior,[8] and distinctive topological spin textures.[9−11] These findings open up exciting possibilities for both fundamental physics research and the development of future information technologies.[12−15] Achieving ultrafast operation speeds, ultrahigh storage density, low energy dissipation, and nonvolatile information storage technology is crucial for future electronic devices but remains a big challenge. One promising avenue involves utilizing an electric field to control the magnetism of 2D magnets, eliminating the requirement of electron current and thus enabling rapid and localized changes in magnetic properties with minimal energy dissipation.[2,16−18] Nevertheless, traditional methods of magnetic control through an electric field rely on a continuous external electric field, resulting in volatile information storage.

The construction of multiferroic van der Waals heterojunctions using 2D magnets and a ferroelectric (FE) gate offers an alternative strategy.[19−21] Examples can be found in systems such as $Cr_2Ge_2Te_6/In_2Se_3$[22] and $MnSeTe/In_2Se_3$[23] heterojunctions. The synergetic effect among Rashba spin−orbit coupling, electronic reconstruction, and others at the interfaces enables the modulation of magnetic interactions,[3,24] thus resulting in the generation of magnetic phases which are absent in the pristine building blocks. Nevertheless, due to the fixed bistable structures typically found in FE materials, achieving the desired magnetism and interconversion between different magnetic phases is not straightforward as the magnetic order depends on the delicate balance among exchange interaction, single-ion anisotropy, and Dzyaloshinskii−Moriya interaction (DMI).[9,25,26] Consequently, exotic magnetic phases such as spontaneous magnetic skyrmions are still rarely reported.[27−29] By employing materials with diverse polarizations, various interactions are altered under different polarization states, thereby facilitating the transition among different magnetic phases and supporting multistate storage and computation. Notably, quadruple-well ferroelectricity, which is the coexistence of four polarization states, was reported in layered bulk $CuInP_2S_6$, offering increased degrees of freedom to address diverse application requirements.[30] However, the quadruple-well property of $CuInP_2S_6$ diminishes substantially when considering few-layer configurations,[31] thereby rendering it less conducive for the generation of 2D magnetic multistates.

Here, based on density functional theory (DFT) calculations, we report that the quadruple-well ferroelectricity can

Received: December 7, 2023
Revised: February 2, 2024
Accepted: February 5, 2024
Published: February 9, 2024

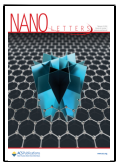

https://doi.org/10.1021/acs.nanolett.3c04799
Nano Lett. 2024, 24, 2345−2351

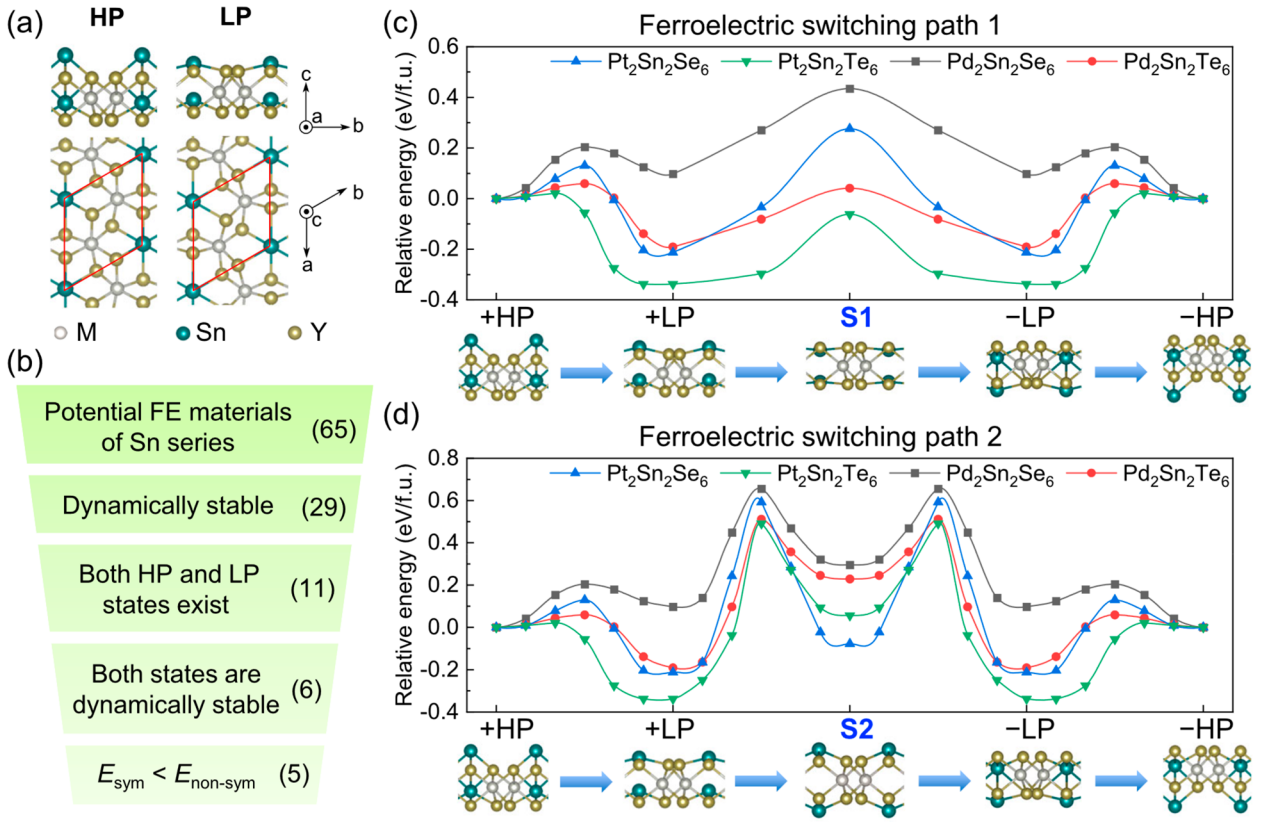

Figure 1. (a) Side and top views of $M_2Sn_2Y_6$ under high and low polarization. (b) Workflow for screening quadruple-well FE materials. (c) and (d) show two possible FE switching paths within FE $M_2Sn_2Y_6$ monolayers. In path 1, two Sn atoms in one unit cell move together, resulting in a transition through high polarization, low polarization, and centrosymmetric S1 states. Alternatively, in path 2, the centrosymmetric state changes to S2, in which the two Sn atoms are out of the MY surfaces. These curves show quadruple-well characteristics. According to the relative energies, switching barriers for path 1 are 0.489, 0.276, 0.336, and 0.232 eV/f.u. for $Pt_2Sn_2Se_6$, $Pt_2Sn_2Te_6$, $Pd_2Sn_2Se_6$, and $Pd_2Sn_2Te_6$, respectively, while those for path 2 are 0.804, 0.828, 0.558, and 0.703 eV/f.u.

persist down to the monolayer limit. We identify four 2D materials, namely, monolayer $Pt_2Sn_2Se_6$, $Pt_2Sn_2Te_6$, $Pd_2Sn_2Se_6$, and $Pd_2Sn_2Te_6$, exhibiting such a remarkable property due to distinct Sn atom displacements. We then construct a heterojunction with FE $Pt_2Sn_2Te_6$ and ferromagnetic CrI_3 due to the small lattice mismatch and also the large SOC effect. By manipulating interfacial-coupling-induced DMI through FE switching and interlayer sliding, we successfully generate diverse magnetic states. The underlying Fert−Levy mechanism explains the induced DMI, offering fundamental insights into the emergence of these intricate magnetic phenomena. Remarkably, a regular skyrmion lattice persists even after the removal of an external magnetic field, demonstrating nonvolatile control over the magnetic skyrmion and other magnetic configurations. This research extends our comprehension of multistate materials and holds immense potential for advancing magnetic structures, with applications spanning nonvolatile spintronics and magnetic devices.

To achieve multistate control over magnetism by FE polarization, we first use high-throughput calculations to screen potential 2D FE materials with quadruple-well FE properties. The hypothesis that quadruple-well ferroelectricity can persist down to the monolayer limit is inspired by a recent discovery of intrinsic scale-free FE $M_2X_2Y_6$.[32] Upon examination of the geometric structures of these $M_2X_2Y_6$, it is found that the extent of the X-X dimer displacement is the outcome of a delicate interplay between the X-X distance and the size of the surrounding skeleton; i.e., the materials tend to be FE when the skeleton is too small to accommodate the X-X dimer. In addition, two stable $M_2X_2Y_6$ phases were reported, and one key difference between these two phases is the X-X distance. These phenomena naturally hint at the possibility of obtaining two different FE $M_2X_2Y_6$ phases within the structures with large X atoms and a proper surrounding skeleton (i.e., the one with a larger (smaller) X-X distance corresponds to a high (low) polarization state HP (LP), as shown in Figure 1a).

To verify this hypothesis, we design a screening pipeline to identify new quadruple-well FE materials, as shown in Figure 1b. By scrutinizing 65 potential FE structures with Sn pairs as suggested in the literature,[32] 29 dynamically stable structures are left. Among these structures, 11 structures possess 2 distinct polarization states (both HP and LP states). Subsequent analysis of the phonon dispersions reveals that only 6 exhibit dynamic stability under both polarization states. Specifically, these stable structures are denoted as $M_2Sn_2Y_6$, where M can be Pt or Pd and Y can be S, Se, or Te. Furthermore, we calculate the total energies of these $M_2Sn_2Y_6$ structures under different states as presented in Table S1. Therein, the structure with two Sn atoms inside (outside) the skeleton denotes S1 (S2), as can be seen in the lower middle structure in Figure 1c,d. Except for $Pt_2Sn_2S_6$, which has the S2 ground state, other five structures have FE ground states and thus are identified as quadruple-well candidates. Upon applying biaxial strain ranging from −2% to 2%, $M_2Sn_2Y_6$ (M = Pt, Pd, and Y = Se, Te) retain their initial FE states, while $Pd_2Sn_2S_6$ has a transition from the LP state to the HP state

https://doi.org/10.1021/acs.nanolett.3c04799
Nano Lett. 2024, 24, 2345−2351

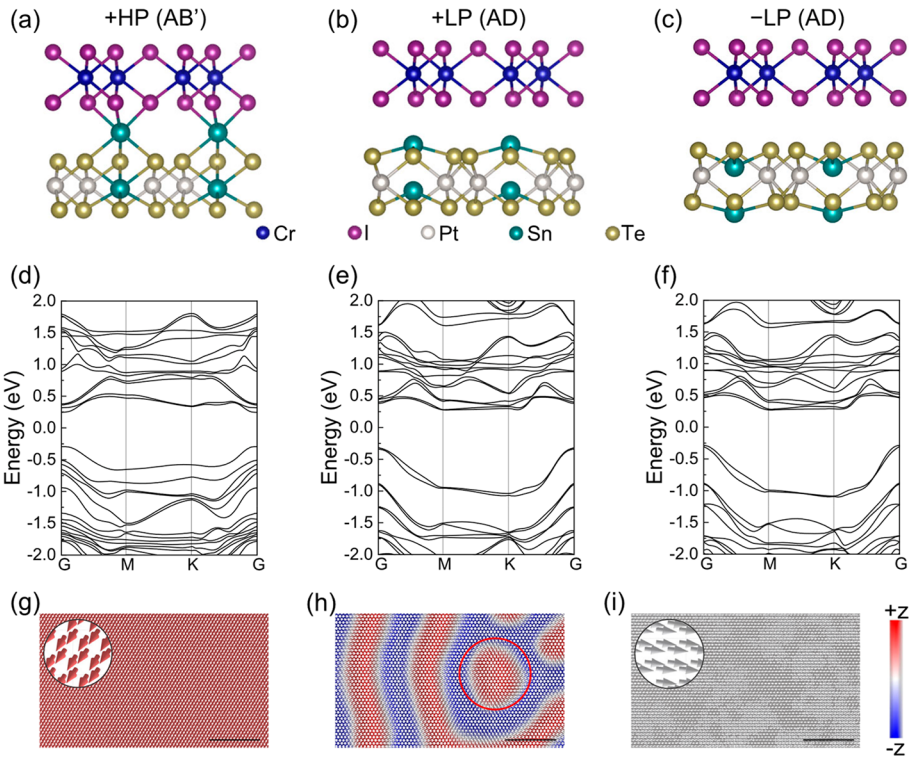

Figure 2. (a−c) Structures of $CrI_3/Pt_2Sn_2Te_6$ heterojunctions at (a) +HP, (b) +LP, and (c) −LP states. For each polarization state, only the structure with the lowest energy is presented. (d−f) Band structures of the three heterojunctions in (a−c). The HSE06 hybrid functional has been used in these calculations considering the SOC effect. (g−i) Monte Carlo simulations of magnetic configurations for the three heterojunctions in (a−c). The black scale bar corresponds to 10 nm. For the +LP state, there is a spontaneously emerged Bloch-type skyrmion with a diameter of 12 nm highlighted by the red circle.

under small compression, which is thus not considered in subsequent discussions. Their total energies under biaxial strain are presented in Figure S1. Their phonon dispersions (Figure S2), ternary phase diagrams (Figure S3), and *ab initio* molecular dynamics simulations (Figure S4) are shown in the Supporting Information, indicating that these materials are dynamically, thermodynamically, and thermally stable.

The band structures of these four materials are obtained using the HSE06 hybrid functional and considering the spin orbit coupling (SOC) effect, as shown in Figure S5, indicating that they are all semiconductors. Their electrostatic potentials under the HP and LP states are shown in Figure S6. The nonzero potential differences verify the existence of FE polarization. Under the HP state, the potential difference is larger than that under the LP state for all the four structures, matching well with their FE polarization results in Table S1. The FE switching paths through both S1 and S2 states are calculated separately. The most intuitive FE switching process is caused by the simultaneously shift of the Sn−Sn pair. This particular FE switching path, labeled as path 1, is illustrated in Figure 1c. Due to the presence of two steady states, namely, HP and LP states, these curves exhibit a unique morphology with four potential wells. Notably, this quadruple-well potential can exist in a single layer, unlike the formation of the quadruple-well potential in $CuInP_2S_6$ that relies on multilayer structure. This discovery marks the first instance that the quadruple-well potential can exist in a single layer. FE switching path 2 corresponds to the transition through the S2 state. In this path, one Sn atom moves first while the other remains motionless. As this transition state is also a metastable state, these potential energy curves as a whole have one more minimum than those in path 1, as shown in Figure 1d. Since path 1 has a lower barrier as compared to path 2, it is thus more likely to happen in these materials. Voltages required for FE switching are also estimated, and the results are shown in Table S2. The estimated voltages are comparable to that of $CuInP_2S_6$, indicating that the four FE $M_2Sn_2Y_6$ are experimentally switchable. We further explore how the FE polarization changes with an increasing number of layers. Figure S7 illustrates the geometric structures of trilayer $Pt_2Sn_2Te_6$, while Table S3 provides information on their relative energies and polarizations. It can be seen that Sn atoms tend to be located in the middle of the two layers with the increase in layers, making the structure symmetrical. Consequently, the polarization does not exhibit a linear increase with the number of layers. The polarizations of bilayer and trilayer structures in the same state are similar. The largest change compared to the monolayer is about 3.6 $pC{\cdot}m^{-1}$ in $Pt_2Sn_2Se_6$, which is still less than that of the monolayer (4.326 $pC{\cdot}m^{-1}$). Eventually, the polarization diminishes in the bulk form due to the centrosymmetric structure.

In the literature, it has been observed that different polarization states hold potential to regulate the magnetic characteristics of other substances.[23] To this end, the ferromagnetic semiconductor CrI_3 has been identified as a promising candidate for regulation due to its experimental synthesis and extensive research background. As a representative FE material, $Pt_2Sn_2Te_6$ is selected due to the lattice mismatch of less than 5% with CrI_3 under both HP and LP states, and also the large SOC effect of the heavy Te and Pt atoms. For each polarization state, eight distinct stacking arrangements have been examined, as presented in Figure S8.

https://doi.org/10.1021/acs.nanolett.3c04799
Nano Lett. 2024, 24, 2345−2351

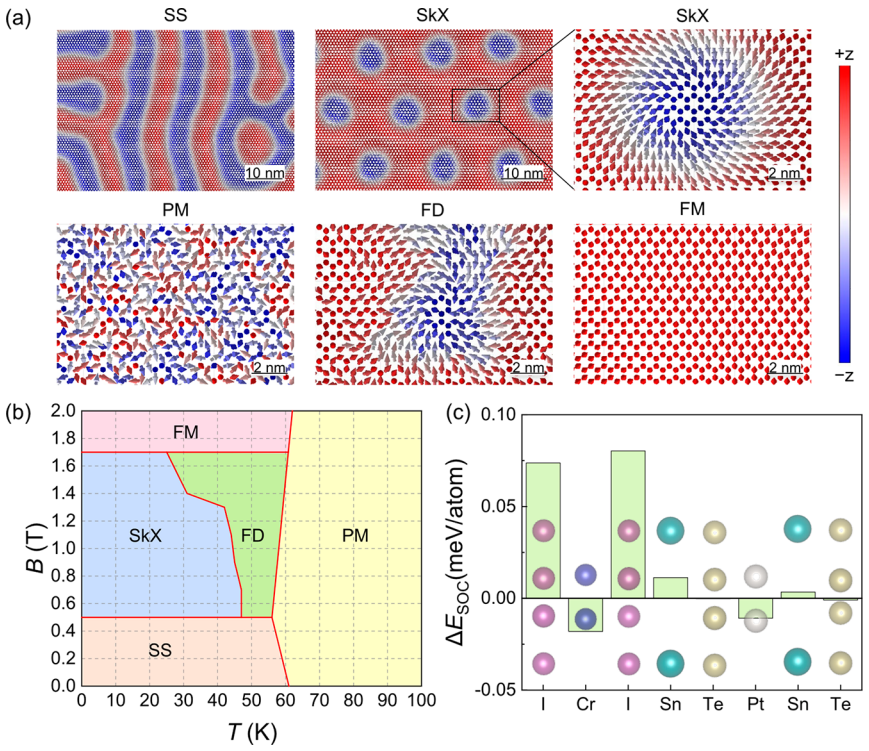

Figure 3. Magnetic configurations of $CrI_3/Pt_2Sn_2Te_6$ heterojunctions with AD stacking in the +LP state. (a) Schematic diagrams of different phases appearing in the MC simulations. (b) Magnetic phase diagram with temperature (T) and external magnetic field (B). (c) Atomic-layer-resolved localization of the DMI-associated SOC energy (ΔE_{SOC}). ΔE_{SOC} is dominated by heavy atom I.

Using a Sn atom as the baseline, it can be located at four unequal high-symmetry points. According to the orientation of the triangle formed by Te atoms, two structures can be formed at each high-symmetry point. When Te atoms form an inverted triangle, structures are labeled by AA, AB, AC, and AD, otherwise AA′, AB′, AC′, and AD′. We find that −HP states for all the stacking models are unstable due to the depolarization effect.[33,34] The relative energies under the three polarization states are summarized in Table S4.

Structures with the lowest energy for each stacking mode are shown in Figure 2a−c. The band structures of these three heterojunctions, incorporating the effect of SOC and employing the HSE06 hybrid functional, are illustrated in Figure 2d−f. It is evident that all the three heterojunctions exhibit semiconducting behavior. Under the +HP state, the band gap of the heterojunction increases substantially, as demonstrated by the projected density of states (Figure S9). The charge density differences in Figure S10 show substantial electron redistribution at the interface, suggesting a strong interaction between CrI_3 and $Pt_2Sn_2Te_6$. Therefore, the increased band gap originates from the strong interlayer interaction.

The computation of the exchange interaction parameter J and single-ion anisotropy A is crucial for understanding their magnetic configurations. The labels of Cr atoms in different locations are depicted in Figure S11. The computed values of J and A for each Cr atom are presented in Tables S5 and S7, with all data assuming $s = 1$. Notably, $A_{zz} - A_{xx} < 0$ for CrI_3 indicates an out-of-plane magnetization, consistent with previous findings.[35,36] Parallel tempering Monte Carlo (MC) simulations are employed to explore the magnetic configurations of these heterojunctions using the Hamiltonian

$$H = \sum_{i,j} \mathbf{S}_i \cdot J_{ij} \cdot \mathbf{S}_j + \sum_i \mathbf{S}_i \cdot A_{ii} \cdot \mathbf{S}_i - \sum_i \mathbf{B} \cdot \mathbf{S}_i$$

where $\mathbf{B}$ represents the external magnetic field. All MC simulations are gradually cooled from 300 K to the investigated low temperature. MC simulations surprisingly show that the magnetic moments under each FE state align in different directions. For the +HP state in AB′ stacking, magnetic moments align along the I−Cr−I direction, as shown in Figure 2g, while for the −LP state in AD stacking, magnetic moments align in-plane, along the x direction, as shown in Figure 2i. When the directions of the magnetic moment are set along these directions, the calculated total energies are shown in Table S8. The energies indicate that the Hamiltonian can accurately describe the magnetic interactions of these systems. It is noteworthy that under the +LP state of $CrI_3/Pt_2Sn_2Te_6$ with AD stacking, spin spiral (SS) characteristics are observed. Most of the magnetic configurations are striped, in which there is a spontaneously emerged Bloch-type skyrmion, as labeled by the red circle in Figure 2h. These distinct electronic bands and magnetic configurations indicate the high tunability of 2D magnets via a suitable FE gate.

Upon increasing the external magnetic field for $CrI_3/Pt_2Sn_2Te_6$ with AD stacking, a regular skyrmion (SkX) lattice phase arises with a period of around 15 nm. The paramagnetic (PM) phase is ascertained by high temperature, while the fluctuation-disorder (FD) phase represents transition states between SkX and PM phases. The criterion employed to determine the transition from the SkX phase to the FD phase is the blurring of skyrmions' boundaries. Distinctive phase illustrations are shown in Figure 3a, while Figure 3b presents the phase diagram of the external magnetic field magnitude and temperature, calculated at intervals of 0.1 T and 1 K. To

https://doi.org/10.1021/acs.nanolett.3c04799
Nano Lett. 2024, 24, 2345−2351

explore the mechanism resulting in the skyrmions in the heterojunction, symmetric and antisymmetric exchange interactions are both considered separately as shown in Figure S12. The MC simulation results reveal that the antisymmetric exchange parameter (i.e., the DMI) is the key factor.

To gain further insight into the DMI, we computed the spin orbit coupling energy ΔE_{SOC} contributed by different atoms. As illustrated in Figure 3c, the principal contribution to DMI does not originate from the magnetic Cr atoms but rather from their adjacent I atoms. Despite the nonmagnetic characteristic of the relatively heavy I atoms, they act as effective sites for spin−orbit coupling scattering, which is vital for DMI generation. Notably, larger atomic numbers correspond to stronger SOC, amplifying the resultant DMI effect. This suggests that the Fert−Levy mechanism accurately captures the strength of the DMI.[37] The I−Cr−I configuration can be viewed as noncentrosymmetric due to the interface interaction, supporting this conclusion.

The energy stabilities of the $CrI_3/Pt_2Sn_2Te_6$ heterojunction with other different stacking modes are also evaluated. We find that after relaxation, the initial structures (+LP state of AB/AC stacking and −LP state of AB stacking) exhibit a tendency to form AA stacking structures. The AA stacking structures are thus metastable structures. It is noteworthy that $A_{zz} - A_{xx}$ is observed to be positive in all three FE polarization cases, indicating the presence of magnetization along the in-plane directions. It is observed that heterojunctions associated with the +LP and −LP states possess in-plane ferromagnetism, while in the case of the +HP configuration, the emergence of the SS phase is also observed. However, the magnetic moments are predominantly aligned within the plane. When an external magnetic field is applied, the Bloch-type SkX phase manifests the similar leading mechanism but no regular skyrmion lattice. The corresponding phase diagram can be found in Figure S13.

As reported in the literature,[25] the interface coupling would induce electron reconstruction across the interface, and the higher electron density at the interface leads to higher inversion asymmetry and hence a larger DMI. We calculate charge density differences of the heterojunction under different stacking modes, as shown in Figure S10. Calculation results reveal substantial charge reconstruction at the interface under AA and AB′ stacking with the +HP state, while there is small charge reconstruction at the interface under AD stacking with both +LP and −LP states. Considering that the AD stacking mode is able to generate a spontaneous magnetic skyrmion in the $CrI_3/Pt_2Sn_2Te_6$ heterojunction, the extensive charge reconstruction at the interface does not necessarily guarantee the formation of skyrmions. The alteration of intralayer bonding induced by the interface interaction also plays a significant role in this context.

Stabilization and reversible manipulation, in addition to the generation of skyrmions, are essential technologies for the construction of skyrmion-based 2D spintronic devices. While various forms of skyrmions have been reported in a number of 2D materials, most of them rely on the continuous application of a strong magnetic field, which is a volatile approach. Furthermore, how to reversibly tune the local skyrmions remains unclear. The unique magnetic interactions within our studied multiferroic heterojunction offer promising avenues to address this challenge. As shown in Figure 4a, starting from AD stacking and the +LP state of the $CrI_3/Pt_2Sn_2Te_6$ heterojunction, a regular skyrmion lattice is achieved by low-energy excitation. When the magnetic field is removed, the regular

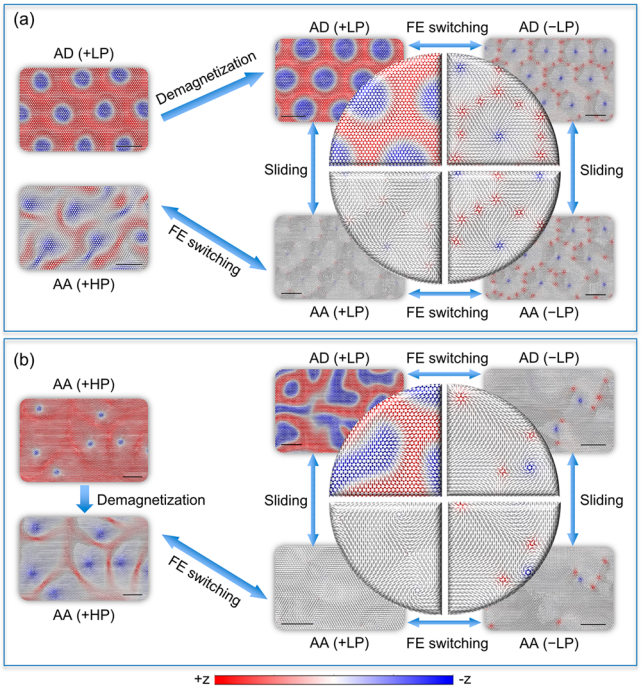

Figure 4. Reversible magnetic configuration evolution for the $CrI_3/Pt_2Sn_2Te_6$ heterojunction as interlayer sliding and FE switching. The black scale bar corresponds to 10 nm. (a) Starting from the AD(+LP) state, the regular skyrmion lattice remains after demagnetization. (b) Starting from the AA(+HP) state, the skyrmions deteriorate after demagnetization.

skyrmion lattice remains. More details can be found in Figure S14. The size of skyrmions becomes larger, consistent with the literature.[38] When the FE polarization state is switched from +LP to −LP under the same AD stacking mode, the Bloch-type skyrmions disappear and a new regular magnetic superstructure arises. In such a magnetic superstructure, each spin vortex along the $-z$ direction is surrounded by multiple spin vortices with the reverse direction. Interestingly, such magnetic topological spin texture cannot be directly obtained by annealing the structure under AD stacking with the LP state. This finding suggests a new approach to discover novel magnetic topological spin textures. Interlayer sliding is another effective approach to tune the magnetic configurations of the $CrI_3/Pt_2Sn_2Te_6$ heterojunction. Under +LP states, when the heterojunction slides from AD stacking to AA stacking, the skyrmions transform to in-plane vortices. Notably, each transform process among these magnetic spin textures is reversible. As a stark contrast, the skyrmions deteriorate dramatically when the magnetic field is removed for the $CrI_3/Pt_2Sn_2Te_6$ heterojunction under the AA stacking mode with the +HP state, as shown in Figure 4b. Spin spirals and spin vortices are also obtained by FE polarization switching or interlayer stacking. The reaction paths associated with polarization change and interlayer sliding for various stacking methods are depicted in Figure S15a−c and Figure S15d,e, respectively. Notably, the barriers along these reaction paths are similar to those reported previously,[32] indicating the feasibility of skyrmion generation, elimination, and manipulation in the $CrI_3/Pt_2Sn_2Te_6$ heterojunction.

The nonvolatile multistate modulation ability of magnetic configurations holds promise for the design of versatile electronic devices. In Figure S16, schematic diagrams depict

https://doi.org/10.1021/acs.nanolett.3c04799
Nano Lett. 2024, 24, 2345−2351

two potential memory devices based on these heterojunctions. Figure S16a illustrates a four-state memory device, highlighting distinct magnetoresistance values associated with different magnetic configurations,[39] enabling the storage of multibit information in a single device. Additionally, Figure S16b showcases the use of skyrmions in racetrack memory, where skyrmions and ferromagnetic gaps represent bits "1" and "0", respectively. These discoveries pave the way for multifunctional devices by integrating magnetic functionalities with other properties. Fundamental physics research also advances with insights into complex magnetic phenomena.

Utilizing first-principles calculations based on DFT, we predict four novel FE 2D materials, namely, $Pt_2Sn_2Se_6$, $Pt_2Sn_2Te_6$, $Pd_2Sn_2Se_6$, and $Pd_2Sn_2Te_6$, with intriguing quadruple potential wells stemming from distinct vertical displacements of Sn pairs. The unique property of these FE materials with various polarization states offer a promising platform to tune the adjacent 2D layers in heterostructures (e.g., 2D magnets via interlayer electromagnetic interactions). A CrI_3/$Pt_2Sn_2Te_6$ heterojunction is then constructed, and its electronic and magnetic properties are investigated. It is found that spontaneous skyrmions and low-energy excited skyrmions can be generated in the heterojunction under AD stacking (+LP) and AA stacking (+HP) modes, respectively. The mechanism for the generation of skyrmions is the Fert−Levy mechanism. Notably, the regular skyrmion lattice for the AD stacking mode persists even after removing the external magnetic field, whereas in the AA stacking mode, it transforms into irregular spin textures. Despite FE switching, interlayer sliding is also an effective approach to reversibly control the skyrmions within these multiferroic heterojunctions. Additionally, we observe an unreported magnetic superstructure characterized by spin vortices with opposite orientations. Our study provides a promising strategy toward nonvolatile control over various magnetic states, showing potentials for generating novel spin textures.

■ ASSOCIATED CONTENT

Supporting Information

The Supporting Information is available free of charge at https://pubs.acs.org/doi/10.1021/acs.nanolett.3c04799.

Computational methods; energy at biaxial strain; phonon dispersions; ternary phase diagrams; AIMD simulations; HSE06 band structures; potential differences; trilayer structures; stacking methods; projected band structures; MC simulations using symmetric and antisymmetric J; phase diagram of the +HP state in AA stacking; charge density differences; demagnetization MC simulations; FE switching and interlayer sliding paths; schematic diagram of potential applications; structure information on $M_2Sn_2Y_6$; estimated voltage for polarization switching; relative energies and related polarizations for different layered cases; energies under different polarization and stacking methods; calculated exchange parameter J, DMI, and single-ion anisotropy A; and relative energies under different magnetic structures (PDF)

■ AUTHOR INFORMATION

Corresponding Authors

Jinbo Pan − *Beijing National Laboratory for Condensed Matter Physics, Institute of Physics, Chinese Academy of Sciences, Beijing 100190, China; School of Physics, University of Chinese Academy of Sciences, Beijing 100049, China; Songshan Lake Materials Laboratory, Dongguan, Guangdong 523808, China*; Email: jbpan@iphy.ac.cn

Shixuan Du − *Beijing National Laboratory for Condensed Matter Physics, Institute of Physics, Chinese Academy of Sciences, Beijing 100190, China; School of Physics, University of Chinese Academy of Sciences, Beijing 100049, China; Songshan Lake Materials Laboratory, Dongguan, Guangdong 523808, China*; orcid.org/0000-0001-9323-1307; Email: sxdu@iphy.ac.cn

Authors

Peixuan Li − *Beijing National Laboratory for Condensed Matter Physics, Institute of Physics, Chinese Academy of Sciences, Beijing 100190, China; School of Physics, University of Chinese Academy of Sciences, Beijing 100049, China*

Lei Tao − *School of Physics, University of Chinese Academy of Sciences, Beijing 100049, China*

Xin Jin − *School of Physics, University of Chinese Academy of Sciences, Beijing 100049, China*

Guolin Wan − *Beijing National Laboratory for Condensed Matter Physics, Institute of Physics, Chinese Academy of Sciences, Beijing 100190, China; School of Physics, University of Chinese Academy of Sciences, Beijing 100049, China*

Jie Zhang − *College of Materials Science and Opto-Electronic Technology, University of Chinese Academy of Sciences, Beijing 100049, China*

Yan-Fang Zhang − *School of Physics, University of Chinese Academy of Sciences, Beijing 100049, China*

Jia-Tao Sun − *School of Information and Electronics, MIIT Key Laboratory for Low-Dimensional Quantum Structure and Devices, Beijing Institute of Technology, Beijing 100081, China*; orcid.org/0000-0003-3519-352X

Complete contact information is available at: https://pubs.acs.org/10.1021/acs.nanolett.3c04799

Notes

The authors declare no competing financial interest.

■ ACKNOWLEDGMENTS

This work was supported by funds from the National Natural Science Foundation of China (61888102, 52102193, 52272172, and 11974045), the Major Program of the National Natural Science Foundation of China (92163206), the National Key Research and Development Program of China (2022YFA1204100 and 2021YFA1201501), and the Fundamental Research Funds for the Central Universities. Computational resources were provided by the National Supercomputing Center in Tianjin.

■ REFERENCES

(1) Dong, X.-J.; You, J.-Y.; Gu, B.; Su, G. Strain-Induced Room-Temperature Ferromagnetic Semiconductors with Large Anomalous Hall Conductivity in Two-Dimensional $Cr_2Ge_2Se_6$. *Phys. Rev. Appl.* **2019**, *12* (1), 014020.

(2) Deng, Y.; Yu, Y.; Song, Y.; Zhang, J.; Wang, N. Z.; Sun, Z.; Yi, Y.; Wu, Y. Z.; Wu, S.; Zhu, J.; Wang, J.; Chen, X. H.; Zhang, Y. Gate-Tunable Room-Temperature Ferromagnetism in Two-Dimensional Fe_3GeTe_2. *Nature* **2018**, *563* (7729), 94−99.

(3) Wang, H.; Liu, Y.; Wu, P.; Hou, W.; Jiang, Y.; Li, X.; Pandey, C.; Chen, D.; Yang, Q.; Wang, H.; Wei, D.; Lei, N.; Kang, W.; Wen, L.; Nie, T.; Zhao, W.; Wang, K. L. Above Room-Temperature Ferromagnetism in Wafer-Scale Two-Dimensional van der Waals

Fe_3GeTe_2 Tailored by a Topological Insulator. *ACS Nano* **2020**, *14* (8), 10045−10053.
(4) Wen, Y.; Liu, Z.; Zhang, Y.; Xia, C.; Zhai, B.; Zhang, X.; Zhai, G.; Shen, C.; He, P.; Cheng, R.; Yin, L.; Yao, Y.; Getaye Sendeku, M.; Wang, Z.; Ye, X.; Liu, C.; Jiang, C.; Shan, C.; Long, Y.; He, J. Tunable Room-Temperature Ferromagnetism in Two-Dimensional Cr_2Te_3. *Nano Lett.* **2020**, *20* (5), 3130−3139.
(5) Lu, J.; Chen, G.; Luo, W.; Íñiguez, J.; Bellaiche, L.; Xiang, H. Ferroelectricity with Asymmetric Hysteresis in Metallic $LiOsO_3$ Ultrathin Films. *Phys. Rev. Lett.* **2019**, *122* (22), 227601.
(6) Yang, Q.; Xiong, W.; Zhu, L.; Gao, G.; Wu, M. Chemically Functionalized Phosphorene: Two-Dimensional Multiferroics with Vertical Polarization and Mobile Magnetism. *J. Am. Chem. Soc.* **2017**, *139* (33), 11506−11512.
(7) Cui, Q.; Liang, J.; Shao, Z.; Cui, P.; Yang, H. Strain-Tunable Ferromagnetism and Chiral Spin Textures in Two-Dimensional Janus Chromium Dichalcogenides. *Phys. Rev. B* **2020**, *102* (9), 094425.
(8) Zhai, Y.; Deng, Y.; Fu, Z.; Feng, E.; Su, Y.; Shiga, T.; Oshio, H.; Zheng, Y. Reentrant Spin Glass and Large Coercive Field Observed in a Spin Integer Dimerized Honeycomb Lattice. *Adv. Funct. Mater.* **2021**, *31* (1), 2004744.
(9) Du, W.; Dou, K.; He, Z.; Dai, Y.; Huang, B.; Ma, Y. Spontaneous Magnetic Skyrmions in Single-Layer $CrInX_3$ (X = Te, Se). *Nano Lett.* **2022**, *22* (8), 3440−3446.
(10) Amoroso, D.; Barone, P.; Picozzi, S. Spontaneous Skyrmionic Lattice from Anisotropic Symmetric Exchange in a Ni-Halide Monolayer. *Nat. Commun.* **2020**, *11* (1), 5784.
(11) Liang, J.; Wang, W.; Du, H.; Hallal, A.; Garcia, K.; Chshiev, M.; Fert, A.; Yang, H. Very Large Dzyaloshinskii-Moriya Interaction in Two-Dimensional Janus Manganese Dichalcogenides and Its Application to Realize Skyrmion States. *Phys. Rev. B* **2020**, *101* (18), 184401.
(12) Kang, W.; Huang, Y.; Zhang, X.; Zhou, Y.; Zhao, W. Skyrmion-Electronics: An Overview and Outlook. *Proc. IEEE* **2016**, *104* (10), 2040−2061.
(13) Finocchio, G.; Büttner, F.; Tomasello, R.; Carpentieri, M.; Kläui, M. Magnetic Skyrmions: From Fundamental to Applications. *J. Phys. Appl. Phys.* **2016**, *49* (42), 423001.
(14) Fert, A.; Reyren, N.; Cros, V. Magnetic Skyrmions: Advances in Physics and Potential Applications. *Nat. Rev. Mater.* **2017**, *2* (7), 1−15.
(15) Nagaosa, N.; Tokura, Y. Topological Properties and Dynamics of Magnetic Skyrmions. *Nat. Nanotechnol.* **2013**, *8* (12), 899−911.
(16) Liu, J.; Shi, M.; Lu, J.; Anantram, M. P. Analysis of Electrical-Field-Dependent Dzyaloshinskii-Moriya Interaction and Magneto-crystalline Anisotropy in a Two-Dimensional Ferromagnetic Monolayer. *Phys. Rev. B* **2018**, *97* (5), 054416.
(17) Jiang, S.; Shan, J.; Mak, K. F. Electric-Field Switching of Two-Dimensional van der Waals Magnets. *Nat. Mater.* **2018**, *17* (5), 406−410.
(18) Huang, B.; Clark, G.; Klein, D. R.; MacNeill, D.; Navarro-Moratalla, E.; Seyler, K. L.; Wilson, N.; McGuire, M. A.; Cobden, D. H.; Xiao, D.; Yao, W.; Jarillo-Herrero, P.; Xu, X. Electrical Control of 2D Magnetism in Bilayer CrI_3. *Nat. Nanotechnol.* **2018**, *13* (7), 544−548.
(19) Gong, C.; Kim, E. M.; Wang, Y.; Lee, G.; Zhang, X. Multiferroicity in Atomic van der Waals Heterostructures. *Nat. Commun.* **2019**, *10* (1), 2657.
(20) Li, Y.; Deng, J.; Zhang, Y.-F.; Jin, X.; Dong, W.-H.; Sun, J.-T.; Pan, J.; Du, S. Nonvolatile Electrical Control of Spin Polarization in the 2D Bipolar Magnetic Semiconductor VSeF. *NPJ. Comput. Mater.* **2023**, *9* (1), 50.
(21) Sun, W.; Wang, W.; Chen, D.; Cheng, Z.; Wang, Y. Valence Mediated Tunable Magnetism and Electronic Properties by Ferroelectric Polarization Switching in 2D FeI_2/In_2Se_3 van der Waals Heterostructures. *Nanoscale* **2019**, *11* (20), 9931−9936.
(22) Li, C.-K.; Yao, X.-P.; Chen, G. Writing and Deleting Skyrmions with Electric Fields in a Multiferroic Heterostructure. *Phys. Rev. Res.* **2021**, *3* (1), L012026.
(23) Jin, X.; O'Hara, A.; Zhang, Y.-Y.; Du, S.; Pantelides, S. T. Designing Strong and Tunable Magnetoelectric Coupling in 2D Trilayer Heterostructures. *2D Mater.* **2023**, *10* (1), 015007.
(24) Zhang, L.; Huang, X.; Dai, H.; Wang, M.; Cheng, H.; Tong, L.; Li, Z.; Han, X.; Wang, X.; Ye, L.; Han, J. Proximity-Coupling-Induced Significant Enhancement of Coercive Field and Curie Temperature in 2D van der Waals Heterostructures. *Adv. Mater.* **2020**, *32* (38), 2002032.
(25) Sun, W.; Wang, W.; Zang, J.; Li, H.; Zhang, G.; Wang, J.; Cheng, Z. Manipulation of Magnetic Skyrmion in a 2D van der Waals Heterostructure via Both Electric and Magnetic Fields. *Adv. Funct. Mater.* **2021**, *31* (47), 2104452.
(26) Cui, Q.; Zhu, Y.; Ga, Y.; Liang, J.; Li, P.; Yu, D.; Cui, P.; Yang, H. Anisotropic Dzyaloshinskii-Moriya Interaction and Topological Magnetism in Two-Dimensional Magnets Protected by P4m2 Crystal Symmetry. *Nano Lett.* **2022**, *22* (6), 2334−2341.
(27) Ba, Y.; Zhuang, S.; Zhang, Y.; Wang, Y.; Gao, Y.; Zhou, H.; Chen, M.; Sun, W.; Liu, Q.; Chai, G.; Ma, J.; Zhang, Y.; Tian, H.; Du, H.; Jiang, W.; Nan, C.; Hu, J.-M.; Zhao, Y. Electric-Field Control of Skyrmions in Multiferroic Heterostructure via Magnetoelectric Coupling. *Nat. Commun.* **2021**, *12* (1), 322.
(28) Yu, G.; Upadhyaya, P.; Li, X.; Li, W.; Kim, S. K.; Fan, Y.; Wong, K. L.; Tserkovnyak, Y.; Amiri, P. K.; Wang, K. L. Room-Temperature Creation and Spin-Orbit Torque Manipulation of Skyrmions in Thin Films with Engineered Asymmetry. *Nano Lett.* **2016**, *16* (3), 1981−1988.
(29) Wiesendanger, R. Nanoscale Magnetic Skyrmions in Metallic Films and Multilayers: A New Twist for Spintronics. *Nat. Rev. Mater.* **2016**, *1* (7), 16044.
(30) Brehm, J. A.; Neumayer, S. M.; Tao, L.; O'Hara, A.; Chyasnavichus, M.; Susner, M. A.; McGuire, M. A.; Kalinin, S. V.; Jesse, S.; Ganesh, P.; Pantelides, S. T.; Maksymovych, P.; Balke, N. Tunable Quadruple-Well Ferroelectric van der Waals Crystals. *Nat. Mater.* **2020**, *19* (1), 43−48.
(31) Duan, X.; Wang, H.; Chen, X.; Qi, J. Multiple Polarization Phases and Strong Magnetoelectric Coupling in the Layered Transition Metal Phosphorus Chalcogenides TMP_2X_6 (T = Cu, Ag; M = Cr, V; X = S, Se) by Controlling the Interlayer Interaction and Dimension. *Phys. Rev. B* **2022**, *106* (11), 115403.
(32) Jin, X.; Tao, L.; Zhang, Y.-Y.; Pan, J.; Du, S. Intrinsically Scale-Free Ferroelectricity in Two-Dimensional $M_2X_2Y_6$. *Nano Res.* **2022**, *15* (4), 3704−3710.
(33) Wurfel, P.; Batra, I. P.; Jacobs, J. T. Polarization Instability in Thin Ferroelectric Films. *Phys. Rev. Lett.* **1973**, *30* (24), 1218−1221.
(34) Mehta, R. R.; Silverman, B. D.; Jacobs, J. T. Depolarization Fields in Thin Ferroelectric Films. *J. Appl. Phys.* **1973**, *44* (8), 3379−3385.
(35) Zhang, W.-B.; Qu, Q.; Zhu, P.; Lam, C.-H. Robust Intrinsic Ferromagnetism and Half Semiconductivity in Stable Two-Dimensional Single-Layer Chromium Trihalides. *J. Mater. Chem. C* **2015**, *3* (48), 12457−12468.
(36) Huang, B.; Clark, G.; Navarro-Moratalla, E.; Klein, D. R.; Cheng, R.; Seyler, K. L.; Zhong, D.; Schmidgall, E.; McGuire, M. A.; Cobden, D. H.; Yao, W.; Xiao, D.; Jarillo-Herrero, P.; Xu, X. Layer-Dependent Ferromagnetism in a van der Waals Crystal down to the Monolayer Limit. *Nature* **2017**, *546* (7657), 270−273.
(37) Fert, A.; Levy, P. M. Role of Anisotropic Exchange Interactions in Determining the Properties of Spin-Glasses. *Phys. Rev. Lett.* **1980**, *44* (23), 1538−1541.
(38) Wang, X. S.; Yuan, H. Y.; Wang, X. R. A Theory on Skyrmion Size. *Commun. Phys.* **2018**, *1* (1), 31.
(39) Huang, Y.; Kang, W.; Zhang, X.; Zhou, Y.; Zhao, W. Magnetic Skyrmion-Based Synaptic Devices. *Nanotechnology* **2017**, *28* (8), 08LT02.

https://doi.org/10.1021/acs.nanolett.3c04799
Nano Lett. 2024, 24, 2345−2351